GEOLOGY | THE GEOLOGICAL SOCIETY OF AMERICA®

https://doi.org/10.1130/G49562.1

Manuscript received 4 April 2021
Revised manuscript received 24 August 2021
Manuscript accepted 26 August 2021

Published online 2 November 2021

The ubiquitous creeping segments on oceanic transform faults

Pengcheng Shi, Meng (Matt) Wei and Robert A. Pockalny
Graduate School of Oceanography, University of Rhode Island, Narragansett, Rhode Island 02882, USA

ABSTRACT

Oceanic transform faults are a significant component of the global plate boundary system and are well known for generating fewer and smaller earthquakes than expected. Detailed studies at a handful of sites support the hypothesis that an abundance of creeping segments is responsible for most of the observed deficiency of earthquakes on those faults. We test this hypothesis on a global scale. We relocate $M_w \geq 5$ earthquakes on 138 oceanic transform faults around the world and identify creeping segments on these faults. We demonstrate that creeping segments occur on almost all oceanic transform faults, which could explain their deficiency of earthquakes. We also find that most of the creeping segments are not associated with any large-scale geological structure such as a fault step-over, indicating that along-strike variation of fault zone properties may be the main reason for their existence.

INTRODUCTION

Oceanic transform faults (OTFs) have long been recognized as hosting fewer and smaller earthquakes than expected (Brune, 1968; Bird et al., 2002). On average, only 15% of the accumulated strain energy on OTFs is released as earthquakes, indicating that most fault slip is accommodated by aseismic creep (Boettcher and Jordan, 2004). Furthermore, accounting for fault step-overs, which lower the accumulated strain energy due to thermal effect and stress interaction (Gregg et al., 2006), only slightly increases the estimate to 18% (Wolfson-Schwehr and Boettcher, 2019).

Four models have been proposed to explain the deficiency of earthquakes on OTFs (Boettcher and Jordan, 2004). The first two are the thin seismogenic zone models where the seismogenic zone is thin and located on either the top or the bottom of the brittle fault area. In these two models, earthquakes occur everywhere along the fault and creeping segments are rare. The third model is the thick seismogenic patch model where most earthquakes occur on a limited number of segments and creeping segments are abundant. In the first three models, the locations of seismic and creeping segments are stationary in time. The fourth model is a multi-modal mechanism where a fault can switch between creeping and seismic slip over time. Differentiating between these models requires both accurate locations of earthquakes and adequately long time windows, which were not available before the early 2000s.

Recent detailed studies, including earthquake relocation and/or ocean bottom seismometer deployments, have been limited to a handful of faults including the Gofar-Discovery faults in the East Pacific Rise (McGuire et al., 2012; Froment et al., 2014), the Blanco fault in the U.S. Pacific Northwest (Braunmiller and Nábělek, 2008), the Eltanin fault in the southeastern Pacific Ocean (Sykes and Ekström, 2012), the Mendocino fault in northern California in the United States (Materna et al., 2018), and the Charlie-Gibbs fracture zone along the Mid-Atlantic Ridge (Aderhold and Abercrombie, 2016). As shown by these studies, the seismic behavior on OTFs is highly segmented, with thick localized seismic and creeping segments having been identified on all these faults. Therefore, Wolfson-Schwehr and Boettcher (2019) proposed that the first two model scenarios with thin seismogenic zones are unlikely, the third model with thick seismogenic patches is most consistent with observations, and the multi-modal model scenario is rare but possible. However, it is still unclear whether their hypothesis is valid for the other >100 OTFs around the world.

We test this hypothesis on a global scale. We relocate $M_w \geq 5$ earthquakes on 138 OTFs. Because most seismic energy is released by large earthquakes on OTFs (Zielke, 2018), these catalogs are able to capture the main earthquake segmentation pattern. When compared with the International Seismological Center (UK) Engdahl–van der Hilst–Buland (ISC-EHB) catalog (http://www.isc.ac.uk/isc-ehb/; Engdahl et al., 2020) and the U.S. Geological Survey (USGS) catalog (https://data.usgs.gov/datacatalog/), our relocated earthquakes are much more accurately located, supported by a significantly improved alignment with the transform trace (Fig. 1). These accurate locations allow us to quantify along-strike seismic moment release on individual OTFs and therefore to identify creeping and seismic segments. Our results support the thick seismogenic patch model and indicate that the ubiquitous creeping segments could explain the deficiency of earthquakes on OTFs on a global scale. We also find most of the creeping segments are not associated with any large-scale geological structure, indicating along-strike variation of fault zone properties on OTFs may be the main reason of the existence of creeping segments.

DATA AND METHODS

For the first time on a global scale, we use cross-correlation between teleseismic surface waves to relocate OTF earthquakes (McGuire, 2008; Cleveland and Ammon, 2013; Wolfson-Schwehr et al., 2014; Howe et al., 2019). We obtain events from USGS earthquake catalogs between 1 January 1950 and 1 December 2020 (https://earthquake.usgs.gov/earthquakes/search). Only events after 1990 (mostly after 1995) are relocated because an adequate distribution of the global seismic network was not available until 1990.

We assume an R1 Rayleigh wave group velocity of 3.75 km/s. We use waveform data from the Global Seismic Network (https://www.iris.edu/hq/programs/gsn; network code GSN) and GEOSCOPE (http://geoscope.ipgp.fr/networks/detail/G/; network code G) because they provide satisfactory azimuthal coverage. Raw waveforms are truncated using a velocity window of 5 km/s to 3 km/s and are bandpass filtered (zero phase) between 0.02 Hz and 0.04 Hz. Cross-correlation between two events yields several differential times at stations of different azimuths. A cosine fitting from azimuths to differential times gives the relative distance, the azimuth,

CITATION: Shi, P., Wei, M., and Pockalny, R.A., 2021, The ubiquitous creeping segments on oceanic transform faults: Geology, v. XX, p. , https://doi.org/10.1130/G49562.1

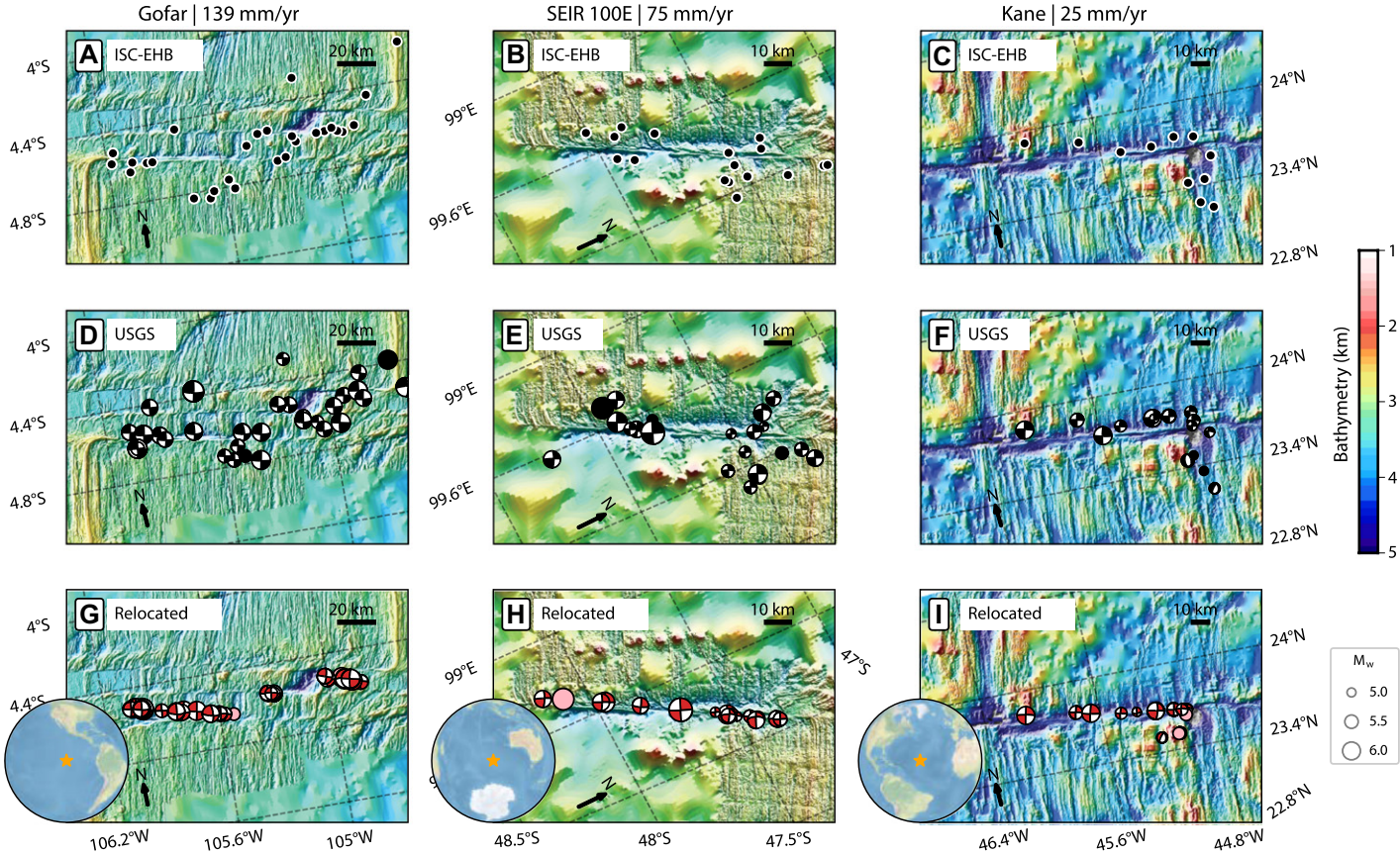

Figure 1. Comparison among International Seismological Center (UK) Engdahl–van der Hilst–Buland (ISC-EHB) catalog locations (A–C), U.S. Geological Survey (USGS) catalog locations (D–F), and corresponding relocated M_w ≥5 earthquakes from this study (G–I) in map view on the Gofar (East Pacific Rise), SEIR 100E (southeast Indian Ridge), and Kane (Mid-Atlantic Ridge) oceanic transform faults. The slip rate of each fault is denoted after its name at the top of the figure. In A–C, the ISC-EHB catalog does not contain events after 2017 and moment magnitude is not available for each event, therefore the number of earthquakes may not match with those of the other panels and they are plotted in uniform black circles. In D–I, an event is marked by a focal mechanism if available from the USGS catalog; otherwise by solid circle. Sizes of earthquake symbols scale with magnitude. Color scale denotes bathymetry.

and their uncertainties between an event pair. Such information is then passed through chains of event pairs to collectively relocate all events in the clusters. Finally, the cluster is shifted depending on the availability of accurate hydroacoustic catalogs or on the geological features from high-resolution bathymetry data (Pan et al., 2002). Additional details on the methodology are provided in the Supplemental Material[1].

To quantify the slip mode of each OTF, first we calculate the subsurface rupture length for each earthquake based on Wells and Coppersmith (1994). Although this method is derived from continental transform earthquakes, this approach (Fig. S1 in the Supplemental Material) is consistent with the well-recorded 2008 M6.0 earthquake on the Gofar OTF (McGuire et al., 2012) and the 2015 M7.1 earthquake on Charlie-Gibbs OTF (Aderhold and Abercrombie, 2016). Second, we assume the along-strike moment release of each earthquake follows an elliptic-shape distribution over the calculated subsurface rupture length based on the elastic crack model (Scholz, 2019). Creeping segments are defined as segments with <10% of the observed maximum moment rate. Then we compute the proportion of total creeping segment length to total fault length, below referred as creeping segment fraction (CSF). We also compute the expected moment rate $\dot{M}_E = \mu A_T V/L$, where the shear modulus, μ, is assumed to be 30 GPa, V denotes the fault slip rate, L is the total fault length, and A_T is the fault area above the 600°C reference isotherm (Boettcher and Jordan, 2004). This estimate serves as a coarse comparison with our computed moment rate curve. Limitations of our method are discussed below.

RESULTS

Using the Gofar OTF as an example, our procedure identifies several creeping segments on the fault (Fig. 2). At a regional scale, Gofar is divided into three segments separated by intra-transform spreading centers, namely G1, G2, and G3 from east to west, following McGuire (2008). At a local scale, five creeping segments are identified by low moment rate, denoted by shaded rectangles in Figure 2C. The average moment rate over the whole time range (since 1950) is significantly lower than the one using relocated events, which is primarily due to the catalog incompleteness before 1990. The similarity of the spatial variation between the two moment rate curves (relocated events only versus all events including non-relocated events since 1950; Fig. 2C) reflects that the earthquake repeating interval on Gofar is relatively short (~5–6 yr), and therefore the time window after 1990 is sufficient to capture its long-term fault behavior. We estimate that 45% of the fault is creeping using the relocated events since 1990 and 15% if using events since 1950. This latter estimate might be an underestimation because non-relocated locations have large errors and appear more scattered along strike, thus smoothing the moment rate curve. Furthermore,

[1]Supplemental Material. Additional information regarding the methods and data, and complete creeping segment fraction results on each oceanic transform fault. Please visit https://doi.org/10.1130/GEOL.S.16811995 to access the supplemental material, and contact editing@geosociety.org with any questions. Code and all relocating results are available online at the Zenodo repository (https://doi.org/10.5281/zenodo.4646438).

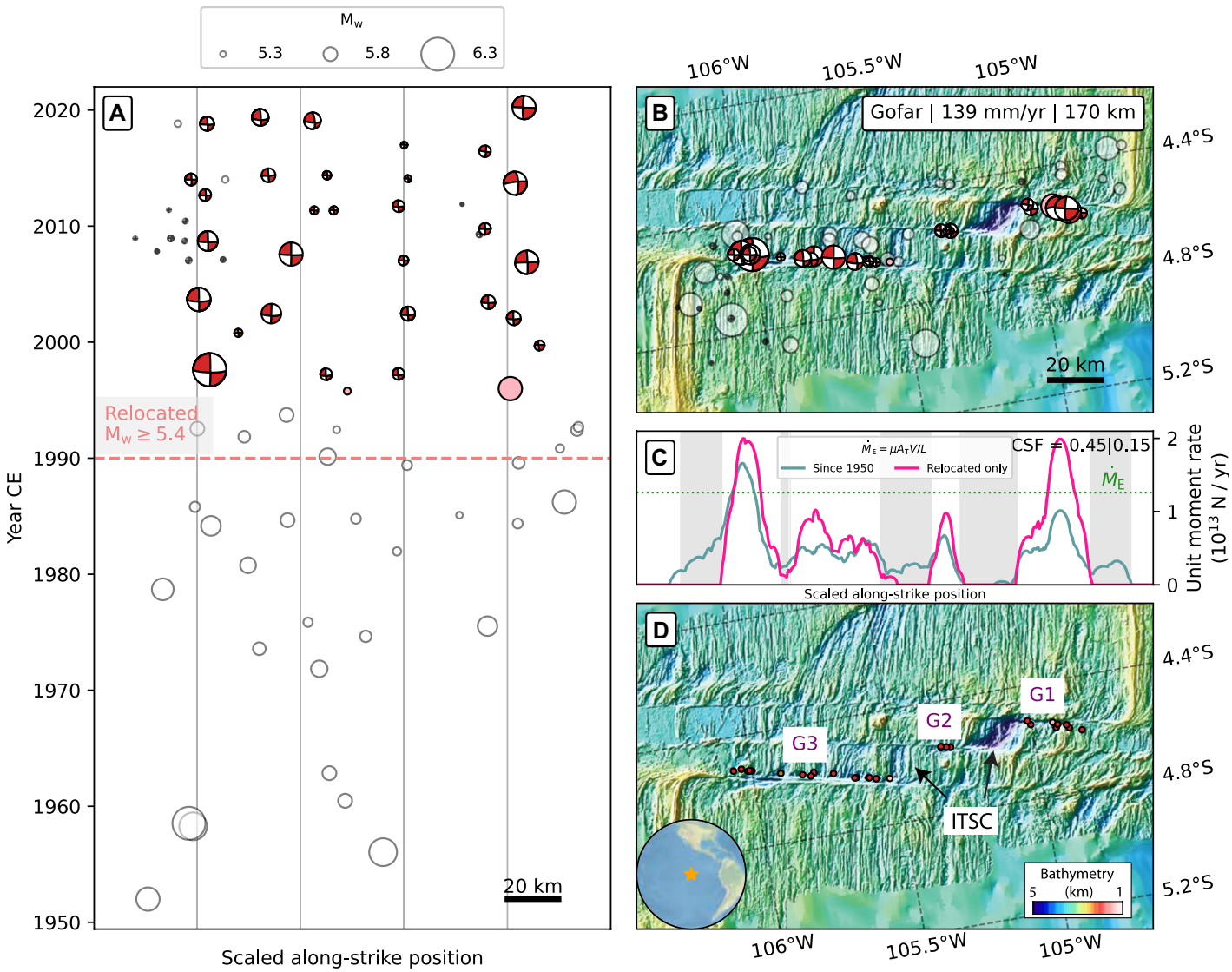

Figure 2. Relocation results on the Gofar oceanic transform fault (East Pacific Rise). (A) Occurrence time versus scaled along-strike position, which corresponds to the map view on the right. The scaled along-strike position means that data have the same relative *x*-axis positions as in panels B and D. Relocated events are colored red if they have focal mechanisms, and colored pink otherwise. Non-relocated events are plotted in semi-transparent gray if they have focal mechanisms, or hollow circles otherwise. Size of the focal mechanisms scales with magnitude. The reference event for translating the whole event cluster from the hydroacoustic catalog (provided by Robert Dziak and Andy Lau [Oregon State University] via personal communication) is annotated. (B) Map view of both relocated and non-relocated earthquakes in a rotated-pole projection. The fault slip rate (139 mm/yr) and the fault length (170 km) are shown for the Gofar OTF. (C) Moment rate curve averaged on different time scales and event groups: pink for only relocated events, and blue for all events after 1950. In both cases, events with explicit non-transform focal mechanisms (rake angle >25°) are excluded. Gray rectangles denote areas of moment rate <10% of the observed maximum. Green dotted line denotes expected moment rate $M_E = \mu A_T V/L$, where μ denotes shear modulus and is assumed to be 30 GPa, A_T is the thermal contact area based on the half-space cooling model from Boettcher and Jordan, (2004), V is the fault slip rate, and L is the total fault length. The creeping segment fraction (CSF) denotes the ratio of the length of fault segments where the moment release is less than 10% of the maximum to the total fault length. The two CSFs correspond to the two moment rate curves using relocated events only, and all events since 1950, respectively. (D) Map view of relocated events (solid red dots). Three distinct segments (G1–G3) as well as the intra-transform spreading center (ISTC) are annotated.

non-relocated events are epicenters instead of epi-centroids, which conforms better with moment release.

Creeping segments, which are defined above as having <10% maximum observed moment rate, are present on almost all OTFs and occupy more than half of the fault length on 100 out of the 138 OTFs (Fig. 3; Table S1). The majority of the OTFs are creeping significantly (Figs. 3C and 3D). The CSF, defined above as the ratio of total creeping segment length to total fault length, on 138 OTFs is on average 64% and ranges from 19% to 100% using relocated earthquakes. The average is 49% if also including events since 1950. Our results do not exhibit geographical clustering of the CSFs; in other words, the CSFs can vary substantially even within the same spreading system (Fig. 3A). We do not observe obvious correlations between CSFs and plate rate or fault length (Fig. 3B), which is consistent with previous work (Boettcher and Jordan, 2004).

The ubiquitous creeping segments could explain the deficiency of earthquakes on OTFs on a global scale. Using relocated events, 65% of the accumulated length of OTFs is creeping. In this study, assuming 0% of the accumulated energy is released as earthquakes in creeping segments, and 50% on the other segments, the global average is 17%. Using events since 1950, the global average is 26%. Both estimates are close to the 18% global average from Wolfson-Schwehr and Boettcher (2019). Therefore, creeping segments

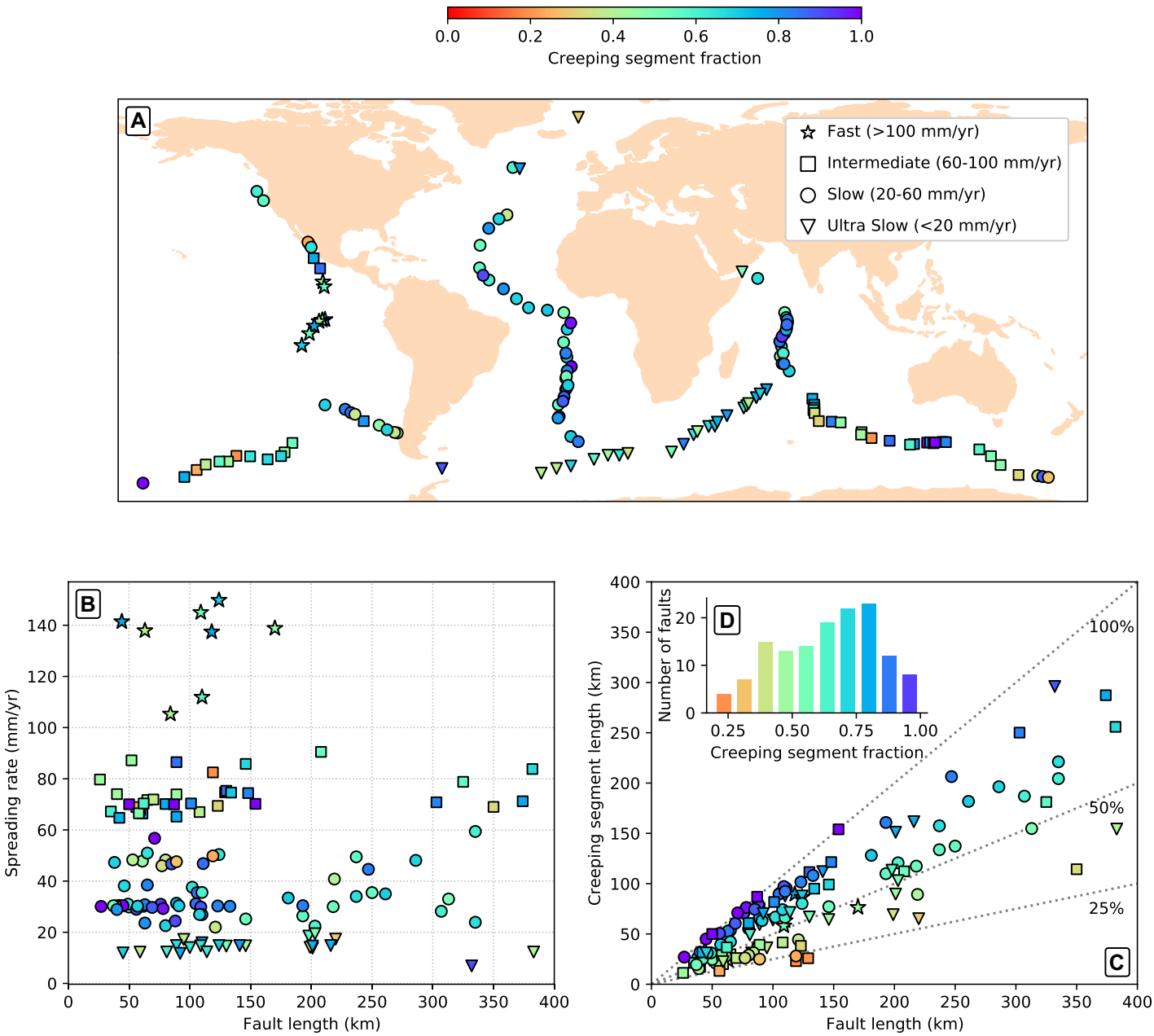

Figure 3. Summary of creeping segment fractions (CSFs) on each oceanic transform fault (OTF) except Sovanco (North Pacific Ocean). (A) CSFs in global map view. Marker type denotes spreading ridge type in terms of the plate rate shown in the top right legend, based on Wanless and Behn (2017). Marker color corresponds to the value of CSF. (B) Relationship between CSF and fault length and plate rate. (C) Distribution of percentage of creeping segment length (dotted lines) versus total fault length. (D) Histogram of CSFs binned by 0.1.

can explain why OTFs generate fewer earthquakes than expected.

Most creeping segments are not associated with any geological structure, which suggests the along-strike variation of fault properties determines whether a fault segment creeps. On 71 OTFs with good bathymetry data, we observe 12 OTFs that have earthquake segmentation delineated by large-scale geological structures (e.g., the Tasman [Tasman Sea], Doldrums [Mid-Atlantic Ridge], and Romanche [central Atlantic Ocean] OTFs). On the other hand, one or more creeping segments are identified within the other 59 OTFs (four examples are shown in Figure 4) as well as within a single straight fault zone segment on OTFs with overlying structural segmentation (e.g., the Gofar segment G3 [Chile], and St. Paul OTF [central Atlantic Ocean]). The seismic moment rate on certain segments of these faults is similar to or above the expected rate based on thermal models (e.g., Fig. 4). These patterns, although with uncertainties (Aderhold and Abercrombie, 2016), best resemble that of the thick seismogenic patch model with localized seismic and creeping segments (Boettcher and Jordan, 2004). Moreover, the number and the relative positions of those creeping segments within the transform trace vary randomly across different OTFs on a global scale. These indicate that along-strike variation of fault zone properties on OTFs may be the main reason for the existence of creeping segments.

DISCUSSION

Our study is the first to relocate large earthquakes on OTFs on a global scale. We also for the first time examine the previously proposed slip models (Boettcher and Jordan, 2004) on OTFs jointly with good bathymetry data on a global scale. Although lacking the same level of detail as near-field seismic studies, our results support the thick seismogenic patch model

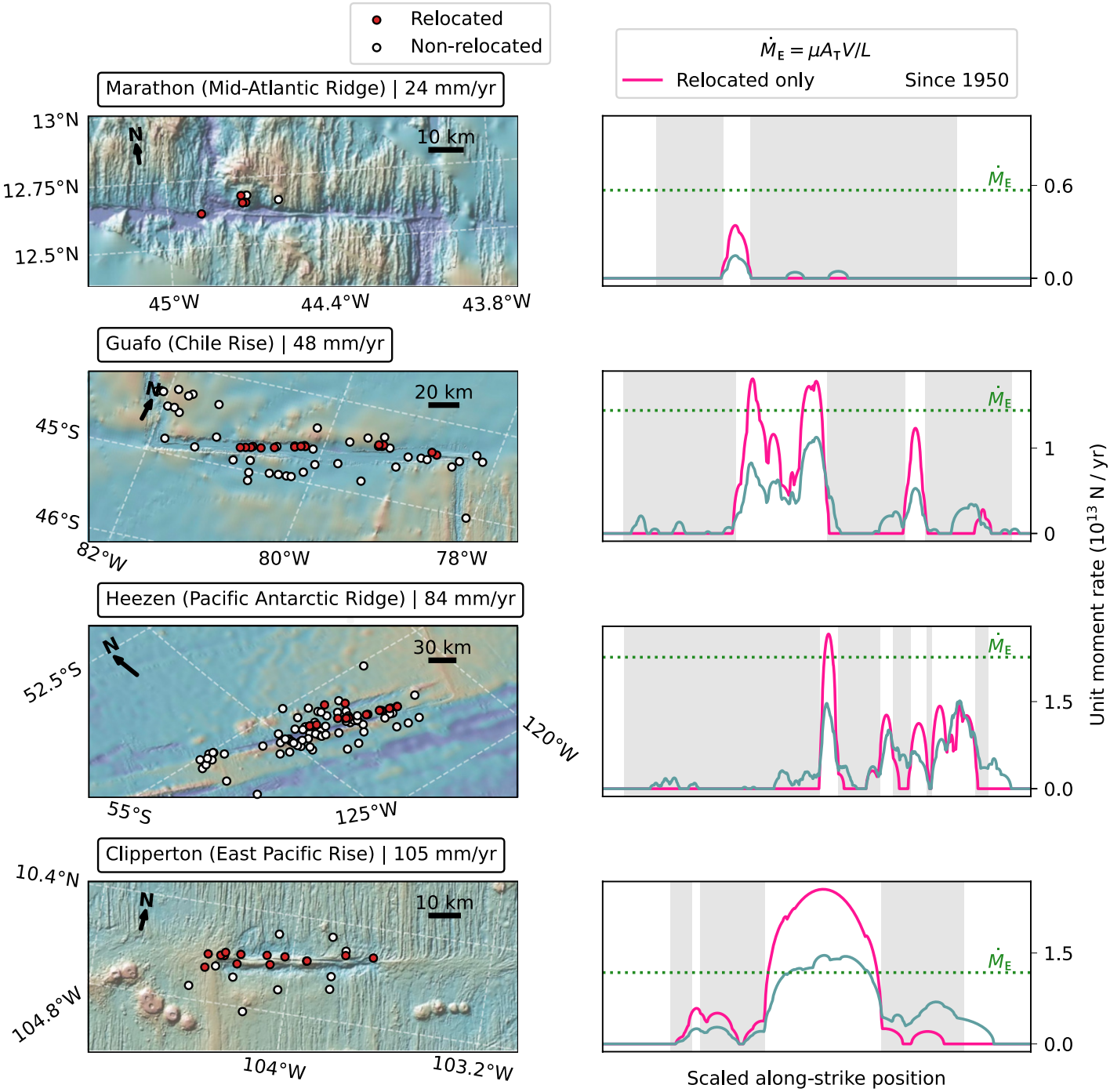

Figure 4. Left panels: Map views of selected faults with different spreading rates and creeping segments not associated with a geological structure. The fault name, its geographic location, and its slip rate are annotated above each map. Red circles are relocated earthquakes and white circles are non-relocated earthquakes. Right panels: Moment rate curves averaged on different time scales and event groups: pink for only relocated events, and blue for all events after 1950. In both cases, events with explicit non-transform focal mechanisms (rake angle >25°) are excluded. Scaled along-strike positions correspond to the x-axis positions of the map views on the left. Gray rectangles denote areas of moment rate <10% of the observed maximum. Green dotted lines denote expected moment rate, $\dot{M}_E = \mu A_T V/L$, where μ denotes shear modulus and is assumed to be 30 GPa, A_T is the thermal contact area based on the half-space cooling model from Boettcher and Jordan, (2004), V is the fault slip rate, and L is the total fault length. Bathymetry base map was obtained with GeoMapApp (http://www.geomapapp.org) by Ryan et al., (2009).

proposed by Boettcher and Jordan (2004) and indicate that the ubiquitous creeping segments can explain the deficiency of OTF earthquakes on a global scale. Even though our results do not explain why OTFs creep so much, we are a step closer to an answer to this fundamental question.

The main limitation of our method is the relatively short time window of data analyzed, especially for slow-spreading OTFs where the recurrence interval of the largest earthquakes is longer than our relocation time window. Therefore, we compute CSFs by using only relocated events and by also including USGS events after 1950 that are not relocated. The latter helps us to avoid mistakenly identifying a seismic segment as a creeping segment if no large events occurred between 1990 and 2020. Such examples include the 15°20′ (Mid-Atlantic

Ridge), Atlantis II (southwest Indian Ocean), and Doldrums OTFs. Even though these OTFs have a lower CSF value in general than other seismically active OTFs, our main observation that creeping segments are abundant on OTFs does not change. As the time span of observations increases, we should see much more robust results using the same approach.

Wolfson-Schwehr and Boettcher (2019) also suggested that multi-modal mechanisms might exist on OTFs, with the strongest evidence being large earthquakes occurring infrequently in the zones of medium to low coupling on the western Blanco OTF (Braunmiller and Nábělek, 2008). We do observe this type of behavior on some faults, such as the Quebrada OTF (South Pacific Ocean). However, this is rare. For faults with short recurrence intervals, most seismic segments rupture regularly as large earthquakes and most creeping segments have not produced any large earthquakes since 1995. For faults with long recurrence intervals, testing whether a multi-modal mechanism is common on OTFs would require a much longer time window of data.

CONCLUSIONS

We relocate $M_w \geq 5$ earthquakes on 138 OTFs around the world and quantify creeping segments on them. We observe that 64% of the accumulated length of OTFs is creeping if using relocated events. The existence of these creeping segments alone can explain the deficiency of earthquakes on OTFs. On a global scale, the thick seismogenic patch model (Boettcher and Jordan, 2004) is most consistent with the observed ubiquities of creeping segments. On 71 OTFs with good bathymetry data, we observe 59 OTFs having creeping segments not associated with large-scale geological structures. This indicates that along-strike variation of fault zone properties may be the main reason for the existence of creeping segments.

ACKNOWLEDGMENTS

This research is supported by the U.S. National Science Foundation (grant 1654416). We thank Robert Dziak and Andy Lau for providing the hydroacoustic earthquake catalog. We thank Rachel Abercrombie for reviewing an early version of this manuscript. We also thank editor Gerald (Jerry) Dickens, reviewer Whitney Behr, and two anonymous reviewers for their helpful comments and suggestions. We use ObsPy (https://doi.org/10.5281/zenodo.3921997) for data retrieval and preprocessing, and GMT (Wessel et al., 2019) and Cartopy (https://scitools.org.uk/cartopy/docs/latest/) for map-related plotting. Bathymetry data were obtained from the Global Multi-Resolution Topography data synthesis (Ryan et al., 2009).

REFERENCES CITED

Aderhold, K., and Abercrombie, R.E., 2016, The 2015 M_w 7.1 earthquake on the Charlie-Gibbs transform fault: Repeating earthquakes and multimodal slip on a slow oceanic transform: Geophysical Research Letters, v. 43, p. 6119–6128, https://doi.org/10.1002/2016GL068802.

Bird, P., Kagan, Y.Y., and Jackson, D.D., 2002, Plate tectonics and earthquake potential of spreading ridges and oceanic transform faults, *in* Stein, S., and Freymueller, J.T., eds., Plate Boundary Zones: American Geophysical Union Geodynamics Series 30, p. 203–218, https://doi.org/10.1029/GD030p0203.

Boettcher, M.S., and Jordan, T.H., 2004, Earthquake scaling relations for mid-ocean ridge transform faults: Journal of Geophysical Research, v. 109, B12302, https://doi.org/10.1029/2004JB003110.

Braunmiller, J., and Nábělek, J., 2008, Segmentation of the Blanco Transform Fault Zone from earthquake analysis: Complex tectonics of an oceanic transform fault: Journal of Geophysical Research, v. 113, B07108, https://doi.org/10.1029/2007JB005213.

Brune, J.N., 1968, Seismic moment, seismicity, and rate of slip along major fault zones: Journal of Geophysical Research, v. 73, p. 777–784, https://doi.org/10.1029/JB073i002p00777.

Cleveland, K.M., and Ammon, C.J., 2013, Precise relative earthquake location using surface waves: Journal of Geophysical Research: Solid Earth, v. 118, p. 2893–2904, https://doi.org/10.1002/jgrb.50146.

Engdahl, E.R., Di Giacomo, D., Sakarya, B., Gkarlaouni, C.G., Harris, J., and Storchak, D.A., 2020, ISC-EHB 1964–2016, an improved data set for studies of Earth structure and global seismicity: Earth and Space Science, v. 7, e2019EA000897, https://doi.org/10.1029/2019EA000897.

Froment, B., McGuire, J.J., van der Hilst, R.D., Gouédard, P., Roland, E.C., Zhang, H., and Collins, J.A., 2014, Imaging along-strike variations in mechanical properties of the Gofar transform fault, East Pacific Rise: Journal of Geophysical Research: Solid Earth, v. 119, p. 7175–7194, https://doi.org/10.1002/2014JB011270.

Gregg, P.M., Lin, J., and Smith, D.K., 2006, Segmentation of transform systems on the East Pacific Rise: Implications for earthquake processes at fast-slipping oceanic transform faults: Geology, v. 34, p. 289–292, https://doi.org/10.1130/G22212.1.

Howe, M., Ekström, G., and Nettles, M., 2019, Improving relative earthquake locations using surface-wave source corrections: Geophysical Journal International, v. 219, p. 297–312, https://doi.org/10.1093/gji/ggz291.

Materna, K., Taira, T., and Bürgmann, R., 2018, Aseismic transform fault slip at the Mendocino Triple Junction from characteristically repeating earthquakes: Geophysical Research Letters, v. 45, p. 699–707, https://doi.org/10.1002/2017GL075899.

McGuire, J.J., 2008, Seismic cycles and earthquake predictability on East Pacific Rise transform faults: Bulletin of the Seismological Society of America, v. 98, p. 1067–1084, https://doi.org/10.1785/0120070154.

McGuire, J.J., Collins, J.A., Gouédard, P., Roland, E., Lizarralde, D., Boettcher, M.S., Behn, M.D., and van der Hilst, R.D., 2012, Variations in earthquake rupture properties along the Gofar transform fault, East Pacific Rise: Nature Geoscience, v. 5, p. 336–341, https://doi.org/10.1038/ngeo1454.

Pan, J., Antolik, M., and Dziewonski, A.M., 2002, Locations of mid-oceanic earthquakes constrained by seafloor bathymetry: Journal of Geophysical Research, v. 107, 2310, https://doi.org/10.1029/2001JB001588.

Ryan, W.B.F., et al., 2009, Global Multi-Resolution Topography synthesis: Geochemistry Geophysics Geosystems, v. 10, Q03014, https://doi.org/10.1029/2008GC002332.

Scholz, C.H., 2019, The Mechanics of Earthquakes and Faulting (third edition): Cambridge, UK, Cambridge University Press, 519 p., https://doi.org/10.1017/9781316681473.

Sykes, L.R., and Ekström, G., 2012, Earthquakes along Eltanin transform system, SE Pacific Ocean: Fault segments characterized by strong and poor seismic coupling and implications for long-term earthquake prediction: Geophysical Journal International, v. 188, p. 421–434, https://doi.org/10.1111/j.1365-246X.2011.05284.x.

Wanless, V.D., and Behn, M.D., 2017, Spreading rate-dependent variations in crystallization along the global mid-ocean ridge system: Geochemistry Geophysics Geosystems, v. 18, p. 3016–3033, https://doi.org/10.1002/2017GC006924.

Wells, D.L., and Coppersmith, K.J., 1994, New empirical relationships among magnitude, rupture length, rupture width, rupture area, and surface displacement: Bulletin of the Seismological Society of America, v. 84, p. 974–1002.

Wessel, P., Luis, J.F., Uieda, L., Scharroo, R., Wobbe, F., Smith, W.H.F., and Tian, D., 2019, The Generic Mapping Tools version 6: Geochemistry Geophysics Geosystems, v. 20, p. 5556–5564, https://doi.org/10.1029/2019GC008515.

Wolfson-Schwehr, M., and Boettcher, M.S., 2019, Global characteristics of oceanic transform fault structure and seismicity, *in* Duarte, J.C., ed., Transform Plate Boundaries and Fracture Zones: Amsterdam, Elsevier, p. 21–59, https://doi.org/10.1016/B978-0-12-812064-4.00002-5.

Wolfson-Schwehr, M., Boettcher, M.S., McGuire, J.J., and Collins, J.A., 2014, The relationship between seismicity and fault structure on the Discovery transform fault, East Pacific Rise: Geochemistry Geophysics Geosystems, v. 15, p. 3698–3712, https://doi.org/10.1002/2014GC005445.

Zielke, O., 2018, Earthquake recurrence and the resolution potential of tectono-geomorphic records: Bulletin of the Seismological Society of America, v. 108, p. 1399–1413, https://doi.org/10.1785/0120170241.

Printed in USA